



Crack closure effects on fatigue damage ahead of crack tips

Samuel Elias Ferreira^{a,*}, Jaime Tupiassú Pinho de Castro^a, Marco Antonio Meggiolaro^a, Antonio Carlos de Oliveira Miranda^b

^a Pontifical Catholic University of Rio de Janeiro, PUC-Rio, Brazil

^b University of Brasilia, UnB, Brazil

ARTICLE INFO

Keywords:

Fatigue crack closure

Strip-yield model

Effective stress intensity range

Damage accumulation ahead of the crack tip

ABSTRACT

Elber's assumed long ago that the effective stress intensity factor (SIF) range $\Delta K_{eff} = K_{max} - K_{op}$ is the actual driving force for fatigue crack growth (FCG), where K_{op} is the SIF that fully opens the crack, and his idea still is widely used to predict residual lives of cracked components. However, although crack closure can affect the FCG process, the ΔK_{eff} idea cannot explain many of its peculiarities. To try to understand why this happens, the actual K_{op} role in FCG is questioned comparing ΔK_{eff} -based predictions with similar predictions obtained using an alternate model that estimates crack increments assuming they are caused instead by the accumulated damage ahead of the crack tip. To be fair, this damage is calculated by the very same strip-yield mechanics used to calculate K_{op} and ΔK_{eff} , i.e. the deformations predicted by the strip-yield model are used to describe the cyclic strain field ahead of the crack tip as well. Hence, the main goal of this exercise is to compare two different hypotheses for the actual FCG driving force using the same formulation basis. Both models are tested for different materials, constraint factors, and stress to yield strength ratios combinations, considering and neglecting the effect of crack closure. This exercise indicates that the effects of crack closure predicted by the critical damage model can be significantly lower than those predicted by the ΔK_{eff} model.

1. Introduction

Elber identified plasticity induced crack closure (PICC) after experimentally verifying through compliance measurements that fatigue cracks can remain partially closed even under tensile loads [1]. He defined the stress intensity factor (SIF) needed to completely open the crack K_{op} and then supposed that only the part of the load cycle larger than the opening load (when $K > K_{op}$ and the crack tip is fully exposed to the load) could contribute for fatigue crack growth (FCG) [2]. Based on this hypothesis, Elber defined an “effective stress intensity range” ΔK_{eff} ($\Delta K_{eff} = K_{max} - K_{op}$ if $K_{op} > K_{min}$, or $\Delta K_{eff} = \Delta K$ if not) and assumed it would be the actual driving force for FCG, instead of SIF ranges and peaks $\{\Delta K, K_{max}\}$ (or their equivalent $\{\Delta K, R\}$) pairs, where $\Delta K = K_{max} - K_{min}$ and $R = K_{min}/K_{max}$.

Based on these ideas, there are two basically different approaches to model the FCG process, which even seem to be contradictory. The first assumes ΔK_{eff} is the FCG driving force, and the other supposes fatigue cracks are instead driven by $\{\Delta K, K_{max}\}$ combinations. Defenders of the latter usually say that FCG must have two driving forces, the SIF range ΔK and the SIF peak K_{max} , because the incremental FCG process is caused by the superposition of ΔK -induced cyclic (pure fatigue) and

K_{max} -induced static failure mechanisms (which can affect pure fatigue, like fracture and environmentally assisted cracking, EAC). Moreover, both ΔK and K_{max} have two well-defined thresholds ΔK_{th} and $K_{max,th}$, which confirm their driving force status. On the other hand, the opening load K_{op} cannot be a driving force, since it is not associated with any failure mechanism and does not have a threshold. Hence, ΔK_{eff} could not be a FCG driving force either, since it depends on K_{op} .

However, although K_{max} can be a driving force for static brittle failure mechanisms, ΔK cannot be a true FCG driving force either. Indeed, ΔK is a linear elastic (LE) parameter that cannot be directly associated with the cyclic fatigue damage induced ahead of crack tips. Physically speaking, the actual damage that causes FCG must be induced by elastoplastic (EP) strain ranges $\Delta \epsilon$ and by stress peaks σ_{max} associated with them, since by definition the SIF-induced LE strains are reversible, hence cannot cause damage. Hence, the actual FCG driving forces should be the EP strain/stress fields that cause the distribution of $\{\Delta \epsilon, \sigma_{max}\}$ pairs at each point inside the plastic zones (pz) ahead of the crack tips. Anyway, from a practical point of view, most structures spend the major part of their FCG lives at relatively low loads, where ΔK and K_{max} control the pz sizes and shapes. Therefore, in such cases it can be safely said that, albeit indirectly, $\{\Delta K, K_{max}\}$ pairs can act as

* Corresponding author.

E-mail address: samuel.ferreira@petrobras.com.br (S.E. Ferreira).

Nomenclature

a	half crack length	S_U	ultimate strength (MPa)
b	fatigue strength exponent	S_Y	yield strength (MPa)
b_k	dimensions for a partially loaded crack ($k = 1, 2$) (m)	SY-CDM	combined strip-yield critical-damage model
c	fatigue ductility exponent	SYM	strip-yield model
CDM	critical damage model	UL	underload
d	half length of the crack plus the monotonic plastic zone (m)	V	crack surface displacement (m)
d_{cr}	half length of the crack plus the monotonic plastic zone of critical SIF (m)	VAL	variable amplitude loading
D	damage at each i^{th} element ahead of the crack tip	W	M(T) specimen half-width (m)
da/dN	fatigue crack growth rate	w_i	half-width of bar element i (m)
E	Young's modulus of elasticity (MPa)	x, y	Cartesian coordinates
EP	elastoplastic	x_i	coordinate location of the element i starting from the specimen center (m)
FCG	fatigue crack growth	x_{ct}	coordinate location starting from the current crack tip (m)
K	stress intensity factor, SIF (MPa $\sqrt{\text{m}}$)	α	constraint factor: $\alpha = 1$ for plane stress; $\alpha = 1/(1 - 2\nu) \approx 3$ for plane strain
K_C	fracture toughness (MPa $\sqrt{\text{m}}$)	Δa	half crack growth increment (m)
K_{max}, K_{min}	maximum and minimum stress intensity factors (MPa $\sqrt{\text{m}}$)	ΔK	stress intensity factor range (MPa $\sqrt{\text{m}}$)
K_{op}	crack opening stress intensity factor (MPa $\sqrt{\text{m}}$)	ΔK_{eff}	effective stress intensity factor range (MPa $\sqrt{\text{m}}$)
LE	linear elastic	ΔK_{th}	threshold stress intensity factor range (MPa $\sqrt{\text{m}}$)
L_i	length of the element i created by plastic deformation (m)	$\Delta \epsilon_y$	strain range in the y direction (m/m)
L_{cr}	element plastic deformation related to critical SIF (m)	$\Delta \epsilon_{y,eff}$	effective strain range (m/m)
n	total number of bar elements	$\Delta \epsilon_{y,th}$	strain range related to a load equivalent to the ΔK_{th} (m/m)
N	fatigue life for a specific load amplitude range	ϵ_c	Coffin-Manson's fatigue ductility coefficient
OL	overload	$\epsilon_{y,cr}$	critical strain (m/m)
PICC	plasticity induced crack closure	η	material constant, $\eta = 0$ for plane stress and $\eta = \nu$ for plane strain
pz, pz_r	monotonic and reverse (or cyclic) plastic zones	ν	Poisson's ratio
R	load ratio ($\sigma_{min}/\sigma_{max}$ or K_{min}/K_{max})	σ_c	Coffin-Manson's fatigue strength coefficient (MPa)
S_{FL}	flow strength, $S_F = (S_Y + S_U)/2$ (MPa)	σ_{cr}	stress related to the critical SIF (MPa)
SIF	stress intensity factor	σ_j	stress at a segment of the crack surface (MPa)
		$\sigma_{max}, \sigma_{min}$	maximum and minimum applied stress (MPa)

practical FCG driving forces.

Many empirical and semi-empirical models can consider load sequence effects in FCG, some based on the FCG phenomenology and others on idealized mechanisms proposed to explain them [3–20]. In particular, PICC arguments can explain many important load-sequence effects in FCG, such as FCG delays or arrests after an overload (OL), attenuation of OL-induced delays after a subsequent underload (UL), and FCG threshold sensibility to R (at least in non-inert environments). Since such effects are most important to estimate fatigue lives under variable amplitude loads (VAL), it is not a surprise that FCG models based on ΔK_{eff} concepts are still very popular in practice. The most used [6–14] are based on Dugdale-Barenblatt's strip-yield pz estimates [21,22], so such models are called SYMs or strip-yield models here. All SYMs need to estimate K_{op} for calculating FCG rates using a suitable $da/dN = f(\Delta K_{eff})$ rule properly fit to experimental data. Most $f(\Delta K_{eff})$ rules need many data-fitting parameters to reproduce FCG data, but the major difficulty when using ΔK_{eff} -based models for VAL is to calculate precisely the variable K_{op} values.

However, even though PICC can justify and even quantify many important load-order effects [1,2,23,24], its actual significance to FCG is still highly controversial. Indeed, ΔK_{eff} concepts cannot explain many other FCG peculiarities that are as important for FCG predictions, such as:

- (i) delays or arrests after OLs under high R (when fatigue cracks remain always open, since for such loads $K_{min} > K_{op}$);
- (ii) constant FCG rates induced by constant $\{\Delta K, R\}$ but highly variable ΔK_{eff} loadings;
- (iii) cracks arrested at a given R that restart to grow at a lower R under the same ΔK_{eff} , or else
- (iv) FCG threshold insensitivity to R in inert environments.

For further details in such and other ΔK_{eff} limitations, see for instance [25–30]. This fact alone justifies the study of alternative FCG models, like the critical damage models (CDMs) used in this work. Such models assume that fatigue cracks grow by sequentially cutting small volume elements (VE) ahead of their tips, which behave like tiny ϵN specimens and break when they reach the fatigue damage they can tolerate [14–20,25]. This is an attempt to directly use the pair $\{\Delta \epsilon, \sigma_{max}\}$, which can be considered the two true FCG driving forces, as explained above.

However, notice that although critical damage ideas are at least as reasonable as the ΔK_{eff} hypothesis, both are just idealized simplifications of the physical reality that do not consider the entire complexity of the FCG process. Thus, ideally they both always should be verified by suitable tests before being used in practical predictions. Such tests should be experimental whenever possible, but numerical tests can be useful as well. This is the main aim of this work: to evaluate numerically how the opening load K_{op} affects the damage induced ahead of fatigue crack tips according to CDM and ΔK_{eff} concepts.

The major problem in this exercise is how to compare apparently conflicting SYM and CDM concepts in a fair way. To do so, the CDMs studied here use the very same formulation employed in SYMs (originally developed to estimate K_{op}) to estimate the plastic strain ranges inside the pzs that always form ahead of fatigue crack tips. EP displacements ahead of the crack tip predicted by SYM procedures are first transformed into strain ranges and then used to estimate fatigue damage through classic ϵN rules, see [31–33] for details. Such procedures allow the evaluation of crack increments at each load cycle under VAL from the length of the region ahead of the crack tip that reaches the maximum accumulated damage the material can tolerate. Moreover, unlike CDMs based on shifted HRR fields or other assumed EP strain distributions, this approach can explicitly recognize crack closure effects on FCG. It can directly evaluate K_{op} effects on the strain ranges

ahead of the crack tip because both K_{op} and $\Delta\varepsilon$ are obtained from the same mechanics. As a result, the CDM used here can predict FCG without neglecting K_{op} effects, but also without having to use Elber's questionable "cracks that are not fully open cannot sustain further damage" hypothesis. Notice that ΔK_{eff} concepts assume loads $K < K_{op}$ cannot induce fatigue damage albeit Elber's original work shows evidence against this idea [2], since his own data indicate strain changes ahead of the crack tip below K_{op} , as previously discussed in [33].

Since the actual effect of crack closure is a most important issue for practical FCG predictions, the idea here is to quantify how much K_{op} affects the strain range field inside the plastic zones that always follow fatigue crack tips. To do so, first the very same SYM mechanics is used to quantify both the opening load and the EP strain range distribution ahead of the crack tip. Then, the damage field associated with the EP strain field is calculated. Finally, predictions based on ΔK_{eff} and on CDM concepts are compared either considering or neglecting the previously calculated K_{op} effects.

2. The combined strip-yield critical damage model, SY-CDM

The SY-CDM uses the strip-yield displacement field to obtain the cyclic plastic strains needed to estimate the associated damage field ahead of the crack tip. Then, it calculates crack increments from the region adjacent to the crack tip, where the accumulated damage reaches its critical value at each load cycle. This model uses only well-defined cyclic material properties to calculate damage through classical εN rules like Coffin-Manson, SWT, or Morrow (the latter two to recognize K_{max} or R effects). The calculated strain field, and thus the consequent damage field as well, are non-singular, since they recognize crack tip blunting for loads $K > K_{op}$.

The first CDM version uses calculated crack increments to fit the single constant of a McEvily-like FCG rule, which can model all three phases of typical FCG curves recognizing proper threshold and toughness limits, namely $\Delta K_{th}(R)$ and K_C , see [31] for details. The cyclic

damage distribution ahead of the crack tip, which depends on the distance of each VE (or tiny εN specimen) from the crack tip blunted by the load, can be accumulated by the Palmgren-Miner linear damage or by any other suitable rule, defining the critical damage as 1.0 or any other value, see Fig. 1.

The second CDM version eliminates the need for an arbitrary (albeit reasonable) McEvily-like FCG rule, introducing two new (equally reasonable) hypotheses [32,33]. The first assumes that if a fatigue limit exists, then there is a limit strain range related to the SIF threshold range ΔK_{th} below which the crack does not grow. In other words, the FCG threshold ΔK_{th} should induce a maximum strain range (in the y-direction perpendicular to the crack plane) $\Delta\varepsilon_{y,th}$ that does not cause damage, thus does not contribute to the FCG process. The second hypothesis assumes the crack becomes unstable at a maximum plastic strain related to the material (or rather to the component) toughness K_C . This critical plastic strain $\varepsilon_{y,cr}$ is the maximum strain the cracked body can sustain before fracturing.

Both CDMs can estimate FCG without needing any data-fitting parameters measured in actual $da/dN \times \Delta K$ tests, a feature that qualifies them as true prediction tools. The third CDM version, the one used here, introduces several modifications in the second version to improve the algorithm numerical performance and to better deal with VAL, as is described along this text.

Combined SY-CDMs use the very same strip-yield mechanics developed by Newman to estimate ΔK_{eff} from Dugdale-Barenblatt displacement fields [7–10]. However, instead of using ΔK_{eff} into the Forman-Newman's FCG rule [34], they transform those fields into their associated strain fields to calculate crack increments by εN damage accumulation procedures, as detailed described in [31–33,35]. Notice that, even though SY-CDMs do not use directly crack opening loads to calculate damage, the K_{op} value (intrinsically generated by SYM procedures) does affect their predictions for the EP strain fields ahead of the crack tips. In other words, crack closure effects on the cyclic damage field ahead of the crack tip are indeed accounted for by SY-CDMs.

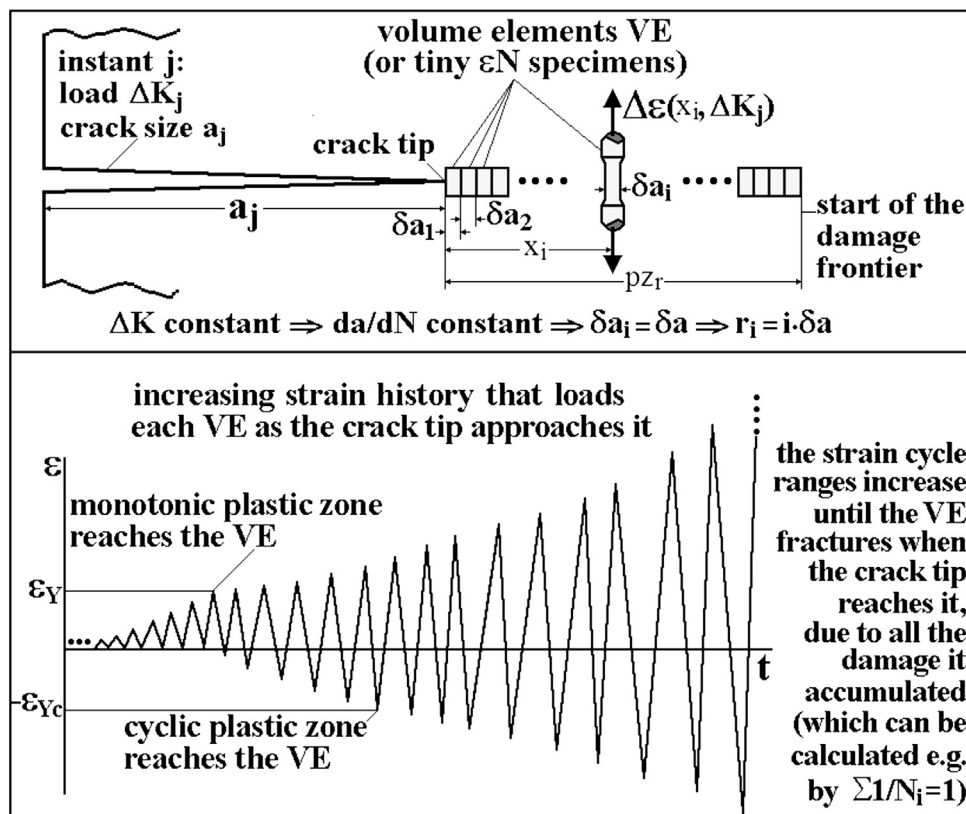


Fig. 1. Schematics of the FCG caused by fracture of a VE at every load cycle [31].

Moreover, the K_{op} importance can be evaluated simply by artificially forcing it to be null both in SY-CDMs and in SYMs. Finally, notice as well that since SYMs and SY-CDMs FCG use the same basic mechanics, their predictions can be fairly and directly compared, in spite of being based on different FCG driving forces.

SYMs and SY-CDMs contain three regions: (i) broken elements along the crack face that keep residual deformations, (ii) unbroken EP elements inside plastic zone, and (iii) the LE part of the residual ligament ahead of the crack tip. The original SYM proposed by Newman, see Fig. 2, leaves residual plastically deformed material around the faces of an advancing fatigue crack. The pz size and residual displacements are obtained by the superposition of two LE solutions for a central cracked plate loaded by (i) a remote uniform nominal tensile stress and (ii) a uniform distributed stress applied over crack surface segments. The plastic zone is discretized in a series of rigid-perfectly plastic 1D bar elements, which are assumed to yield at the flow strength of the material, $S_{FL} = (S_Y + S_U)/2$, to somehow account for the otherwise neglected strain-hardening effects. These elements are either intact at the plastic zone or broken at the crack wake, in this case storing residual plastic deformations. The broken bar elements can carry compressive stresses during unloading and therefore they can yield in compression when their stresses reach $-S_{FL}$. The elements along the crack face that are not in contact do not affect the crack surface displacements, neither carry stresses. These same basic ideas are maintained in the SY-CDMs to allow the fair comparison between theirs and SYMs predictions. Indeed, although it is not too difficult to improve some of the maybe too simplified SYM assumptions (like 1D bar elements and perfectly plastic material), it would not be possible to properly collate SY-CDM and SYM predictions otherwise.

The SYM simulates the effects of the actually 3D stresses around the crack tip, caused by plastic restrictions when the plate is thick (and cannot be assumed to work under plane stress), by using a constraint factor α that increases the tensile flow stress S_{FL} in the unbroken pz elements during the loading. Thus, this constraint factor should vary from $\alpha = 1$ for plane stress up to $\alpha = 1/(1 - 2\nu) \approx 3$ for plane strain limit conditions, where ν is Poisson's coefficient. As there is no crack-tip singularity when the crack closes, in Newman's original model this constraint factor is not applied to unbroken elements inside the pz ahead of the crack tip during unloading, neither to broken elements at the crack wake along the crack faces, a feature kept by the SY-CDM

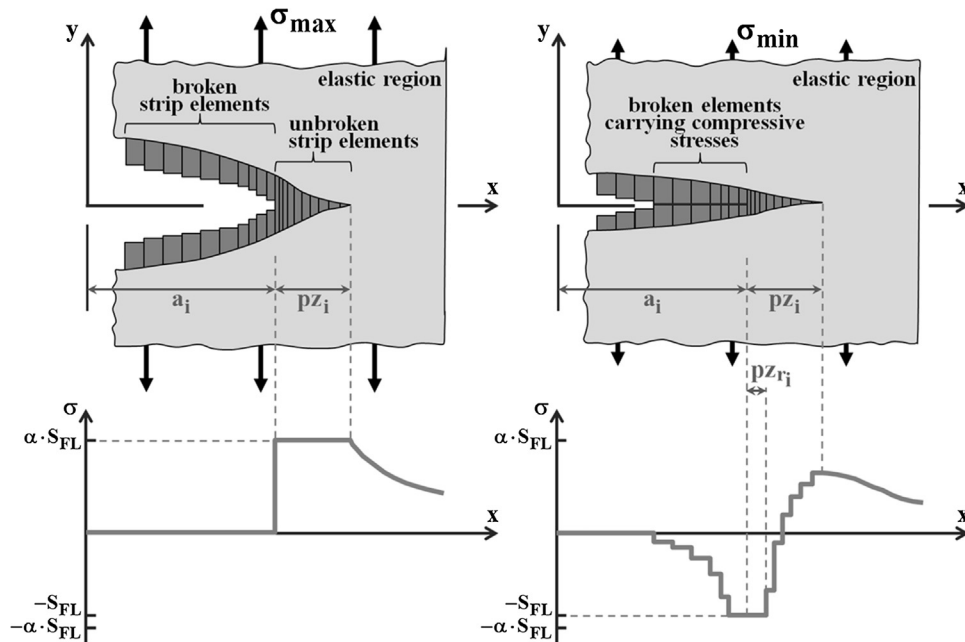


Fig. 2. Crack surface displacements and stress distribution along the crack line [7].

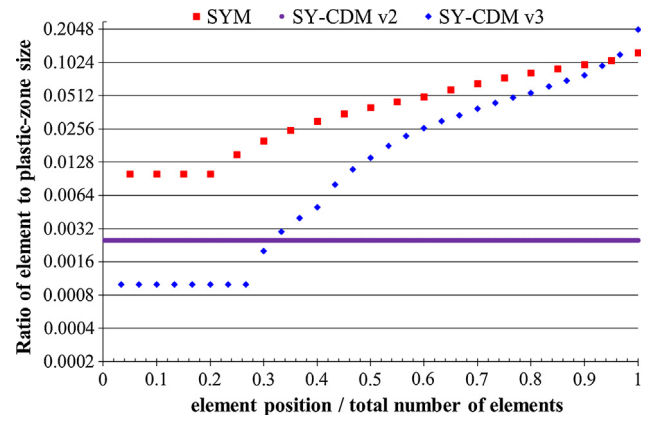


Fig. 3. Ratio between element width and plastic zone size.

used here.

Fig. 2 schematizes the stress distributions in the bar elements at maximum σ_{max} and minimum σ_{min} applied stresses. Displacement and stress fields are obtained from Eq. (1) requiring compatibility between the LE part of the cracked plate and all the bar elements. The influence functions $f(x_i)$ and $g(x_i, x_j)$ are related to the plate geometry and its width correction, as is expressed in Eqs. (2)–(4).

$$V_i = \sigma_n f(x_i) - \sum_{j=1}^n \sigma_j g(x_i, x_j) \tag{1}$$

$$f(x_i) = [2(1 - \eta^2)/E] \cdot \sqrt{(d^2 - x_i^2)} \sec(\pi d/2W) \tag{2}$$

$$g(x_i, x_j) = G(x_i, x_j) + G(-x_i, x_j) \tag{3}$$

$$G(x_i, x_j) = \frac{2(1 - \eta^2)}{E} \left\{ (b_2 - x_i) \cdot \cosh^{-1} \left(\frac{d^2 - b_2 x_i}{d |b_2 - x_i|} \right) - (b_1 - x_i) \cdot \cosh^{-1} \left(\frac{d^2 - b_1 x_i}{d |b_1 - x_i|} \right) + \sqrt{d^2 - x_i^2} \cdot [\sin^{-1}(b_2/d) - \sin^{-1}(b_1/d)] \cdot \left[\frac{\sin^{-1} B_2 - \sin^{-1} B_1}{\sin^{-1}(b_2/d) - \sin^{-1}(b_1/d)} \right] \cdot \sqrt{\sec \left(\frac{\pi d}{2W} \right)} \right\} \tag{4}$$

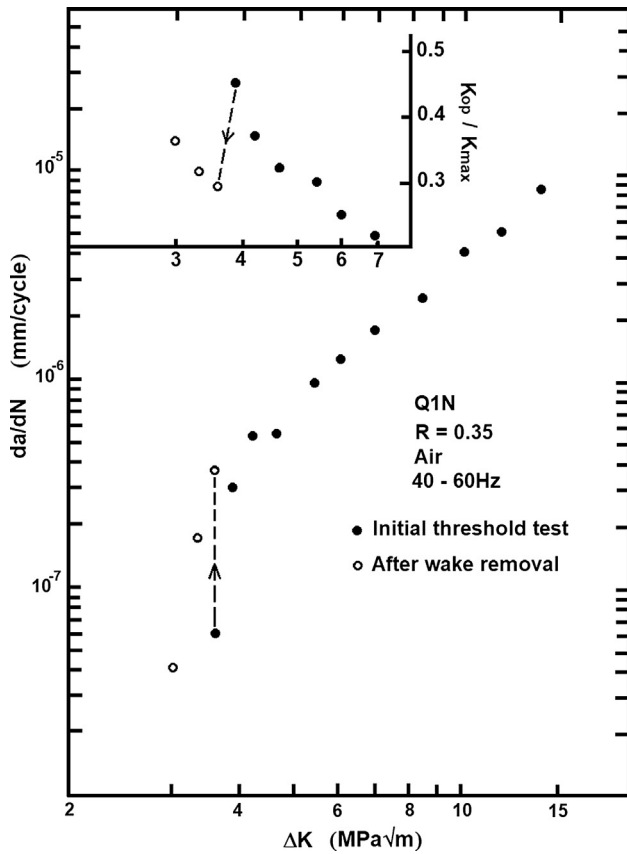


Fig. 4. Effect of removing most of the plastic wake around the crack faces [37].

Table 1
Simulation conditions.

Material	R	α	ΔK_{min} (MPa√m)	ΔK_{max} (MPa√m)
6351-T6	0.1	1	4.09	23.80
		2		38.31
		3		
	0.4	1	3.46	15.87
		2		24.00
		3		
7075-T6	0.1	1	3.47	22.63
		2		
		3		
	0.4	1	3.21	15.09
		2		
		3		
1020	0.1	1	11.83	30.72
		2		40.00
		3		
	0.4	1	9.74	20.43
		2		40.00
		3		

Table 2
Material properties used for the SY-CDM simulations.

Material	S_y (MPa)	S_U (MPa)	ϵ_c	c	K_{IC} (MPa√m)	ΔK_{th} (MPa√m)	
						R = 0.1	R = 0.4
6351-T6	285	318	0.92	-0.53	43	4.01	3.39
7075-T6	498	576	0.12	-0.75	25.4	3.4	3.15
1020	285	491	0.25	-0.54	277	11.6	9.55

Notice that $\eta = 0$ for plane stress and $\eta = \nu$ for plane strain, that B_1 and B_2 are calculated from Eq. (5), and that b_1 and b_2 are edge elements calculated from Eqs. (6) and (7). The width of all elements is $2w = b_2 - b_1$. The monotonic plastic zone is calculated from Eq. (8) for a central cracked plate (called M(T) in ASTM standards) and from Eq. (9) for others geometries [9–10]:

$$B_k = \sin(\pi b_k / 2W) / \sin(\pi d / 2W) \tag{5}$$

$$b_1 = x_j - w_j \tag{6}$$

$$b_2 = x_j + w_j \tag{7}$$

$$pz = a \{ (2W / \pi a) \cdot \sin^{-1} [\sin(\pi a / 2W) \cdot \sec(\pi \sigma_{max} / 2\alpha S_{FL})] - 1 \} \tag{8}$$

$$pz = (\pi / 8) \cdot (K_{max} / \alpha S_{FL})^2 \tag{9}$$

The SYM can deal with input loads given by stresses or by SIFs. Albeit the original formulation is for a cracked plate, it can be adapted for other geometries using the similitude concept, since a similar FCG rate is expected when it is induced by the same SIF in different specimen geometries. Notice that this argument is somehow inconsistent, since the SYM assumes that the actual FCG driving force is ΔK_{eff} , not ΔK , and there is no guarantee that K_{op} is geometry-independent, but SYM users usually neglect this fact. By computing the SIF of an M(T) specimen through Eq. (10), the input stress can be estimated as proposed in [9]:

$$K = \sigma \sqrt{\pi a \sec(\pi d / 2W)} \tag{10}$$

The third version of the SY-CDM presented here discretizes the pz into 30 variable width bar elements, as in the original SYM. Fig. 3 shows the ratio between the element width ($2w$) and the plastic zone size for the SYM and the combined SY-CDM versions 2 and 3. The SY-CDM version 2 (v2) divides the plastic zone into 400 elements with width equivalent to $0.0025 \cdot pz$. In the SY-CDM version 3 (v3) the number of elements is reduced to 30 but, instead of a constant, they have variable widths. The thinnest element has width $0.001 \cdot pz$, ten times smaller than the original SYM ($0.01 \cdot pz$). The introduction of variable width elements in the SY-CDM v3 did not cause relevant numerical differences in a preliminary evaluation presented in [33]. The element configuration of the SY-CDM v3 from Fig. 3 has been tested under several material and load conditions (including VAL) with satisfactory results. However, the change in the number of elements from 400 to 30 has reduced the required computer time by a factor of about 25.

After discretizing the plastic zone and defining the position of the bar elements, the SY-CDM calculates the elements' deformation (L_{max}) under maximum applied stress by Eq. (11), a simple modification of Eq. (1). The results of this equation for the elements at the crack surface represent the displacements at the maximum stress (V_{max}):

$$L_{max} = V_{max} = \sigma_{max} \cdot f(x_i) - \sum_{j=1}^{30} \alpha \cdot S_{FL} \cdot g(x_i, x_j) \tag{11}$$

A similar calculation is performed for a hypothetical load related to the material toughness. As explained above, to avoid the need to use FCG threshold and toughness properties, $\Delta K_{th}(R)$ and K_{IC} , to reproduce the three phases of typical $da/dN \times \Delta K$ curves, two new hypotheses based only on eN principles and on the physics of the FCG process were introduced into the SY-CDM [32,33]. Before estimating the critical plastic strain, it is necessary to calculate the deformations related to the critical SIF as in Eq. (12). The critical deformation is calculated for the same elements used in Eq. (11), i.e. the deformations are calculated at the same position. The functions $f(x_i)$ and $g(x_i, x_j)$ are calculated as described in Eqs. (2)–(4), replacing the variable d by d_{cr} ; the stress σ_{cr} is defined using K_{IC} in the FIT solution of the M(T) specimen, see Eq. (10):

$$L_{cr} = \sigma_{cr} \cdot f(x_i) - \sum_{j=1}^{30} \alpha \cdot S_{FL} \cdot g(x_i, x_j) \tag{12}$$

Under the minimum stress σ_{min} , the elements inside the pz discharge

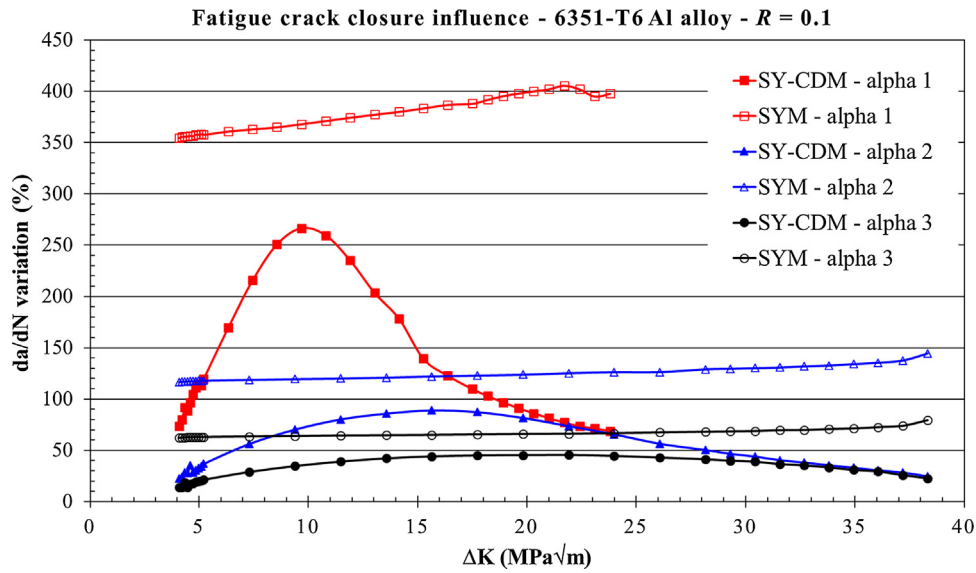


Fig. 5. Fatigue crack closure effect predicted for the 6351-T6 Al alloy at R = 0.1.

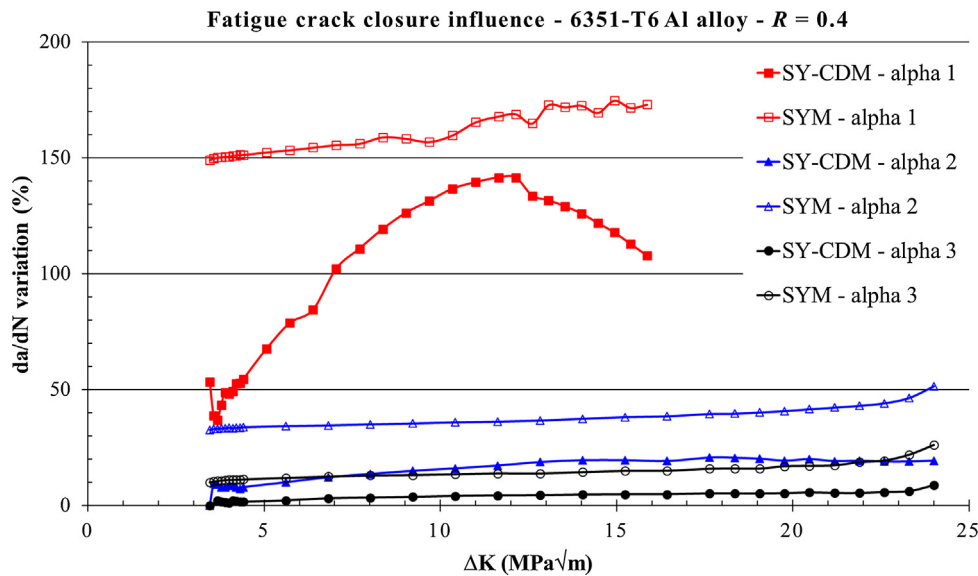


Fig. 6. Fatigue crack closure effect predicted for the 6351-T6 Al alloy at R = 0.4.

until some of them near the crack tip yield in compression when they reach $-S_{FL}$ (during unloading, the constraint factor is $\alpha = -1$ for all elements inside the plastic zone), forming the reverse plastic zone. The broken elements along the crack faces can contact each other during unloading carrying compressive stresses as well. Some of these elements can also yield in compression when their stress reaches $-S_{FL}$. The stress σ_j acting at each element must be identified before calculating their residual plastic deformation. Eq. (1) can be rearranged into Eq. (13), where L_i are the elements deformation from Eq. (11) for $x_i > a$, or the residual plastic deformations for the elements located at the crack wake.

$$\sum_{j=1}^n \sigma_j g(x_i, x_j) = \sigma_{min} f(x_i) - L_i \quad (13)$$

This system of equations is solved by using the Gauss-Seidel method with restraints added, like first proposed in [7]. For the elements inside the plastic zone ($x_j > a$) these restrictions are related to their idealized yield behavior in tension and in compression, as described by Eqs. (14) and (15). For the broken elements located at the crack wake along the crack faces, the restrictions are related to their separation and to

yielding in compression, as expressed by Eqs. (16) and (17).

$$if \sigma_j > \alpha S_{FL} s_0 \sigma_j = \alpha S_{FL} \quad (14)$$

$$if \sigma_j < -S_{FL} s_0 \sigma_j = -S_{FL} \quad (15)$$

$$if \sigma_j > 0 s_0 \sigma_j = 0 \quad (16)$$

$$if \sigma_j < -S_{FL} s_0 \sigma_j = -S_{FL} \quad (17)$$

The solution of Eq. (13) for the stresses σ_i acting in the elements results in Eq. (18), employed by the iterative method, where the index I is the current number of the iteration step. The matrix g_{ij} defined by Eq. (3) has as diagonal the vector g_{ii} and the description of the iterative process can be found in [7]. The iterative process is repeated until the maximum error in the stress vector reaches values below $0.01 \cdot S_{FL}$. This method converges quickly within 3 to 20 iteration steps for the number of elements normally used by the model.

$$(\sigma_i)_I = \left[\sigma_{min} f_i - L_{max} - \sum_{j=1}^{i-1} (\sigma_j)_I g_{ij} - \sum_{j=i+1}^n (\sigma_j)_{I-1} g_{ij} \right] / g_{ii} \quad (18)$$

After finding the stress field, it is possible to calculate the residual

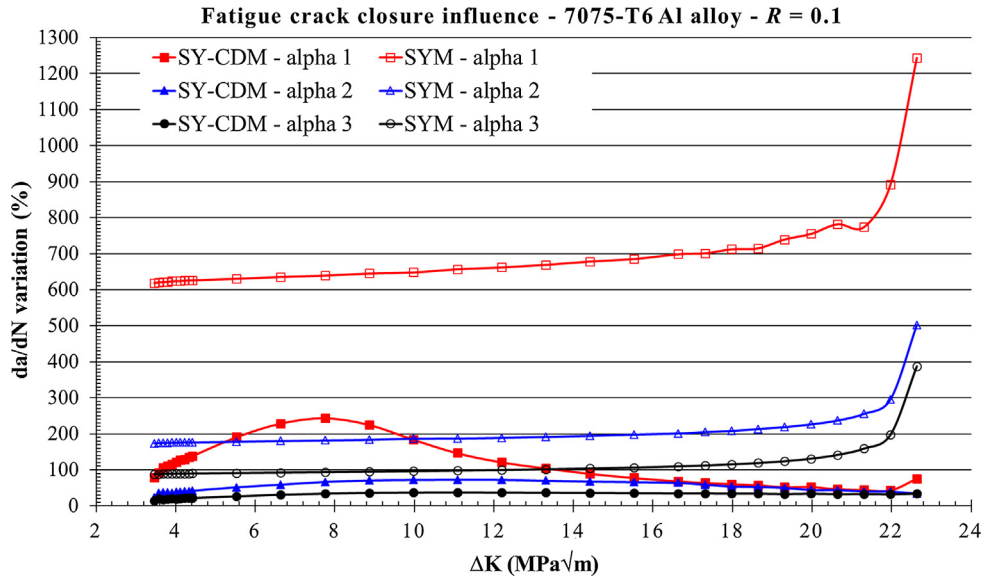


Fig. 7. Fatigue crack closure effect predicted for the 7075-T6 Al alloy at R = 0.1.

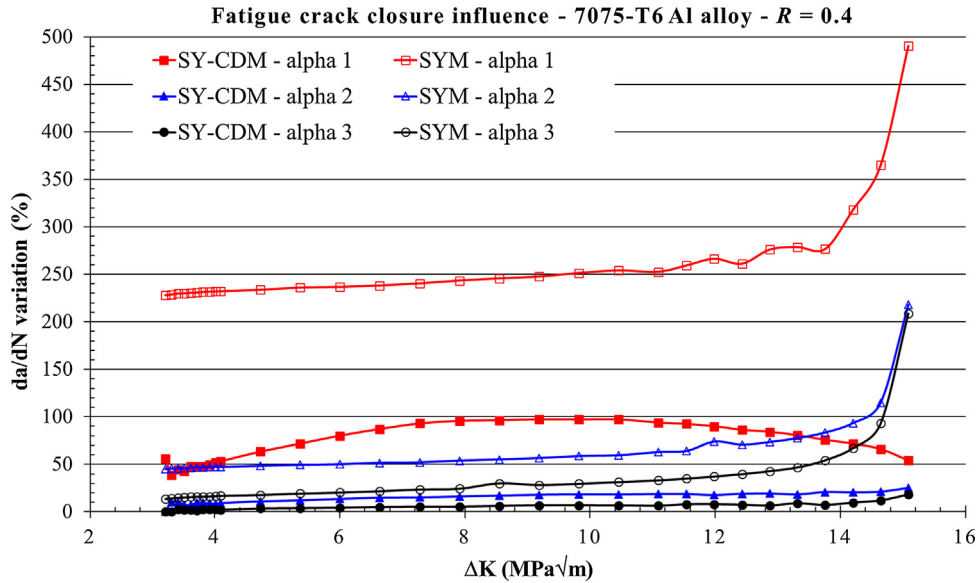


Fig. 8. Fatigue crack closure effect predicted for the 7075-T6 Al alloy at R = 0.4.

plastic deformations at each element that yielded in compression using Eq. (19):

$$L_{min} = V_{min} = \sigma_{min} \cdot f(x_i) - \sum_{j=1}^n \sigma_j \cdot g(x_i, x_j) \quad (19)$$

Another step required in the SY-CDM formulation is the calculation of the plastic deformation due to a stress range related to $\Delta K_{th}(R)$. As fatigue cracks do not propagate when $\Delta K(R) \leq \Delta K_{th}(R)$, the plastic deformations related to $\Delta K_{th}(R)$ cannot induce damage in the material ahead of the crack tip. The first step of the SY-CDM algorithm then defines the load condition due to the FCG threshold as $K_{min,th} = K_{min}$ and $K_{max,th} = K_{min,th} + \Delta K_{th}$. This notation is convenient for the modeling, because it avoids the calculation of plastic deformations under $K_{min,th}$ i.e. $L_{min,th} = L_{min}$.

The computation of plastic deformations ahead of the crack tip due to an applied load equivalent to $K_{max,th}$ is performed with the same elements created for the current load cycle. As K_{max} (or σ_{max}) is always higher than $K_{max,th}$ (or $\sigma_{max,th}$), before computing the plastic deformations it is necessary to find the stress field acting ahead of the crack tip

under an applied $\sigma_{max,th}$ (the stress equivalent to $K_{max,th}$). This is done through Eq. (18), but replacing σ_{min} by $\sigma_{max,th}$ and L_{max} by L_{min} . After getting the stress profile, the next step is to calculate $L_{max,th}$ ahead of the crack tip using Eq. (11), replacing σ_{max} by $\sigma_{max,th}$ and $\alpha \cdot S_{FL}$ by the stress vector σ_i .

Plastic strain ranges ahead of the crack tip are calculated by Eq. (20), derived from the solution proposed by Rice [36] to estimate the plastic strain field of tensile cracks based on their crack tip opening displacements. In Eq. (20), x_{cr} locates the element starting from the current crack tip. Plastic strains related to the critical SIF $\epsilon_{y,cr}$ and to maximum applied stress σ_{max} are calculated by Eqs. (21) and (22). In a similar way, the plastic strain range due to the threshold is obtained from Eq. (23).

$$\Delta \epsilon_y = \log [(L_{max} + x_{ct}) / (L_{min} + x_{ct})] \quad (20)$$

$$\epsilon_{y,cr} = \log (1 + L_{cr} / x_{ct}) \quad (21)$$

$$\epsilon_{y,max} = \log (1 + L_{max} / x_{ct}) \quad (22)$$

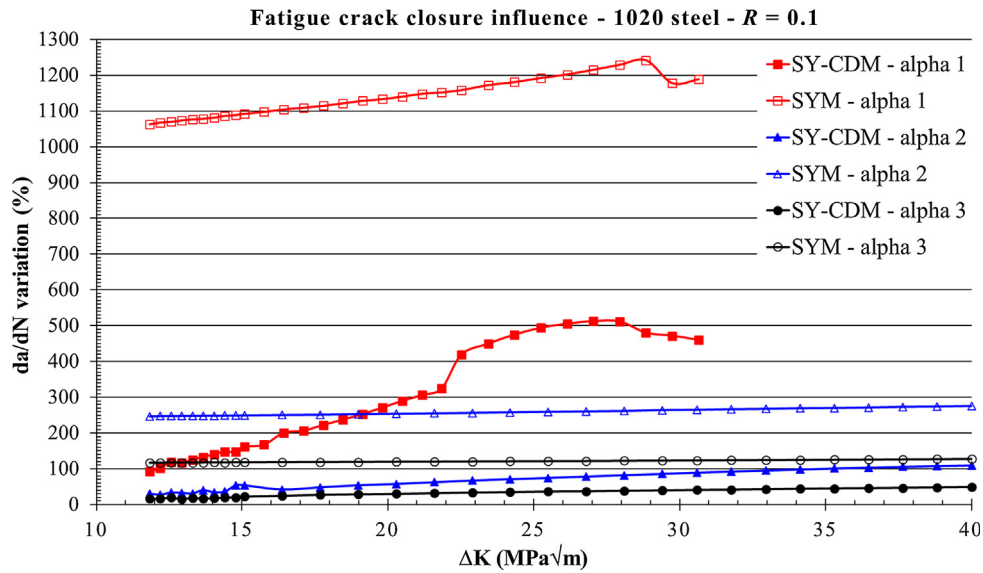


Fig. 9. Fatigue crack closure effect predicted for the 1020 low carbon steel at R = 0.1.

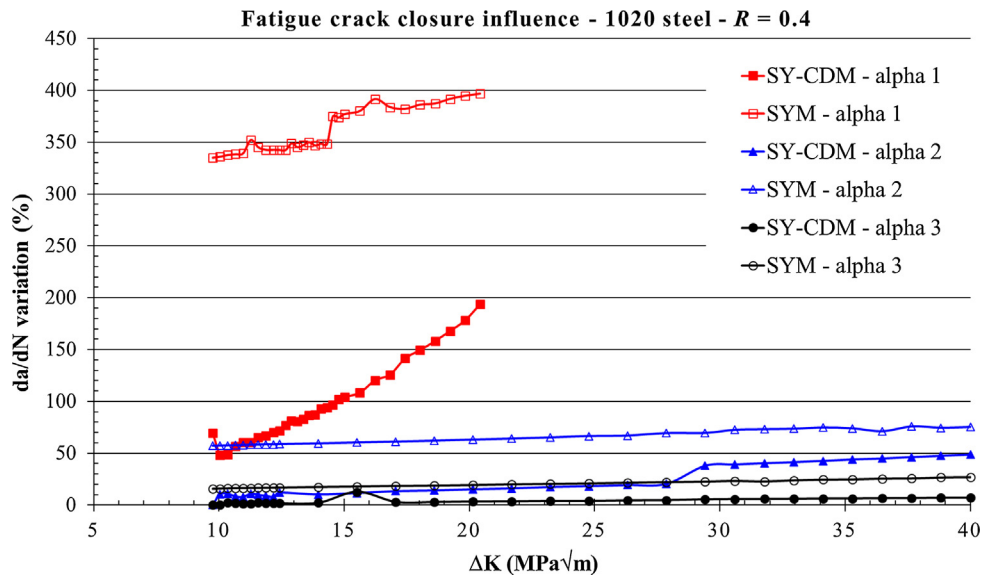


Fig. 10. Fatigue crack closure effect predicted for the 1020 low carbon steel at R = 0.4.

$$\Delta\epsilon_{y,th} = \log [(L_{max,th} + x_{ct}) / (L_{min,th} + x_{ct})] \quad (23)$$

Effective plastic strain ranges that act at the center of each bar element ahead of the crack tip are calculated at each load cycle by Eq. (24). These strain ranges can be correlated with the number of cycles N that would be required to break each element if they were kept constant during its entire life using the plastic part of Coffin-Manson's rule Eq. (25), or of the SWT rule using Eq. (26). Damage at each element D is calculated using Palmgren-Miner's rule, Eq. (27), and the crack increment at each load cycle is defined at the position where the accumulated damage reaches the value of 1.0.

$$\Delta\epsilon_{y,eff} = [\Delta\epsilon_y - \Delta\epsilon_{y,th}] \cdot [\epsilon_{y,cr} / (\epsilon_{y,cr} - \epsilon_{y,max})] \quad (24)$$

$$N = (1/2) \cdot (\Delta\epsilon_{y,eff} / 2\epsilon_c)^{1/c} \quad (25)$$

$$N = (1/2) \cdot (\sigma_{max,i} \cdot \Delta\epsilon_{y,eff} / 2\sigma_c \epsilon_c)^{1/(b+c)} \quad (26)$$

$$D = 1/N \quad (27)$$

As the crack propagates, an interpolation process is required to correctly define the accumulated damage value for the unbroken

elements inside the new plastic zone. At each load cycle a new element is created at the crack surface with the width equivalent to the crack increment and, to avoid a large number of elements, the model uses a lumping process for elements along the crack surface.

All elements located along the crack surface, except for the element n just behind the crack tip, are tested using the criterion presented in Eq. (28). When this criterion is satisfied, two adjacent elements are lumped forming an element of width equal to the sum of the widths of both elements. The residual plastic deformation of the lumped element is calculated using a weighted average, expressed by Eq. (29):

$$2(w_i + w_{i+1}) \leq a - x_{i+1} - 2 \cdot \Delta a \quad (28)$$

$$L = (L_i w_i + L_{i+1} w_{i+1}) / (w_i + w_{i+1}) \quad (29)$$

Notice that all such CDM procedures are coherent with the hypothesis the bar elements ahead of the crack tip behave as tiny ϵN specimens, and their predictions for FCG rates can be easily verified by simply measuring them. Their main advantage is that they use only well-defined Coffin-Manson material properties, i.e. they do not need or use any data-fitting parameter of previous crack growth tests to predict

Table 3
Average FCG rate increments.

Material	R	α	Average FCG rate increment (%)		Ratio SYM/SY-CDM
			SY-CDM	SYM	
6351-T6	0.1	1	129.80	375.78	2.9
		2	47.30	124.51	2.6
		3	30.71	66.41	2.2
	0.4	1	94.56	159.41	1.7
		2	14.33	37.42	2.6
		3	3.64	14.29	3.9
7075-T6	0.1	1	111.15	693.23	6.2
		2	50.82	206.56	4.1
		3	29.50	115.58	3.9
	0.4	1	71.73	259.11	3.6
		2	14.32	64.33	4.5
		3	5.41	35.31	6.5
1020	0.1	1	284.44	1132.53	4.0
		2	66.49	257.56	3.9
		3	31.59	120.91	3.8
	0.4	1	98.20	360.30	3.7
		2	22.40	65.03	2.9
		3	4.04	20.20	5.0

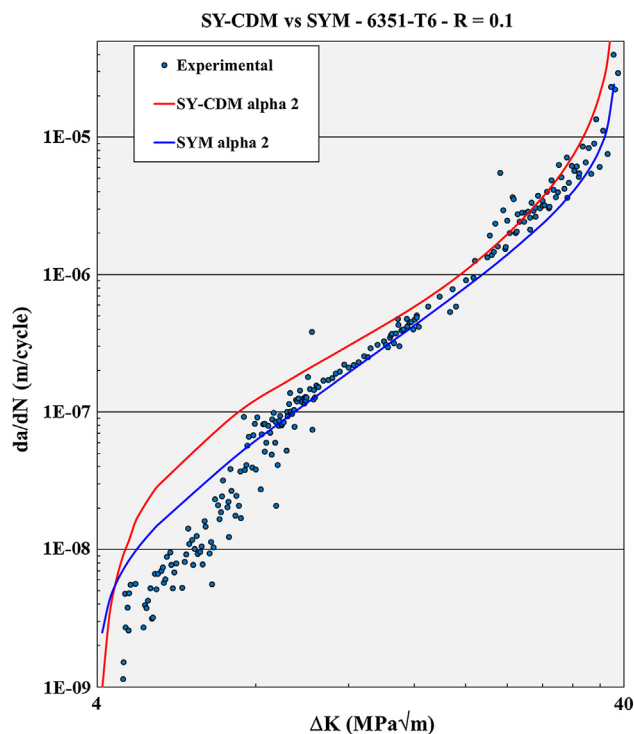


Fig. 11. SY-CDM and SYM predictions for the $da/dN \times \Delta K$ curve of the 6351-T6 alloy at $R = 0.1$, compared with the experimental data measured according to ASTM E647 procedures.

FCG rates. In this sense, knowing the ϵN properties of the material the CDM can really make FCG predictions using only sound mechanical tools.

3. Numerical simulations

James and Knott [37] investigated the intrinsic threshold SIF range of a quenched and tempered Q1N steel, measuring crack-opening loads and FCG rates in four-point bending specimens. They used an electro-discharge machine (EDM) to remove part of the plastic wake around the crack faces, to find the effect of crack closure on the FCG rate. After reaching the threshold in an $R = 0.35$ test, they identified 1.2 mm of

wake-induced closure. Part of this wake was removed by EDM, leaving only 0.5 mm of wake behind the crack tip. Upon restarting the test at the same load, they found that the growth rate was higher and the closure lower than during the previous cycling, see Fig. 4.

The increase in FCG rates after the plastic wake removal is a clear evidence of how crack closure can affect them, but those authors unfortunately did not show whether such rates quantitatively increased as was predicted by ΔK_{eff} . This is a most important point, because even when crack closure exists and can affect FCG rates, the significant question for practical applications is whether its effect can be well predicted when using the ΔK_{eff} approach to model it. That is why the claim “crack opening loads can affect FCG rates” is not disputed here. The point in question is if there is an alternative explanation for K_{op} effects that can be used even when they cannot be quantified by ΔK_{eff} principles.

Previous works have shown that $da/dN \times \Delta K$ FCG curves can be quite well predicted for several materials both by ΔK_{eff} -based SYMs and by CDMs. New data for the 6351-T6 Al alloy presented latter on in this work support this claim. SYMs assume the material follows a Forman-Newman FCG curve with 4 data-fitting parameters, and frequently use a constraint factor as still another data-fitting parameter. CDMs, on the other hand, assume FCG can be modeled by ϵN -based crack initiation and fatigue damage accumulation principles using only the Coffin-Manson properties of the material [31–33]. Those experimental results clearly show there is no need to introduce artificial corrections in basic ϵN tools (like ill-defined size effects or any other data-fitting parameter, for that matter) to achieve or even to improve CDMs predictions.

In particular the SY-CDMs predictions, based on damage accumulated by plastic strain ranges ahead of crack tips calculated by the very same mechanics used by SYMs to estimate K_{op} and ΔK_{eff} , intrinsically include K_{op} effects on their estimated FCG curves. Hence, they can be fairly compared to SYMs predictions. Moreover, it makes sense to estimate FCG rates under fixed $\{\Delta K, R\}$ conditions by SY-CDMs considering and neglecting crack closure to evaluate its effect on such rates (according to CDM principles). It makes sense as well to repeat this exercise with the SYMs predictions. In this way, quantitative estimates for crack closure effects on FCG rates according to critical damage and to ΔK_{eff} principles can be coherently compared. Besides the purely academic appeal, this exercise can provide a quantitative tool to those interested in identifying which are the true FCG driving forces, a must for improving the reliability of residual life prediction models. Indeed, even if such models can be properly fitted to sets of FCG data under VAL, it is at least questionable to use them as prediction tools for different conditions if they are based in wrong driving forces hypothesis.

The effect of crack closure in FCG is evaluated here using the SY-CDM for three materials, 6351-T6 and 7075-T6 Al alloys and 1020 steel, under $R = 0.1$ and $R = 0.4$. Moreover, each material and R calculation uses three different constraint factors ($\alpha = 1, 2$, and 3), to simulate plane stress, plane strain, and intermediate conditions for a wide range of ΔK , as it is listed in Table 1. FCG rates are calculated using Coffin-Manson’s parameters (Eq. (25)) for thirty ΔK points between the limits listed in Table 1, either considering or neglecting crack closure effects for each condition. 360 simulations are performed for each material. FCG rates are also calculated using Newman’s original SYM [7–10] as is described in [34]. Material properties used for FCG rate predictions with the combined SY-CDM are listed in Table 2.

4. Results and discussion

The percent increments of the FCG rate predicted by the SYM and by the SY-CDM for a given R due to the elimination of crack closure effects are presented in Figs. 5 to 10, as a function of the applied SIF range ΔK . The closure effect is evaluated by first calculating the predicted $da/dN \times \Delta K$ rate considering the calculated K_{op} value, and then by artificially forcing it to be null. The results for 6351-T6 Al alloy are shown in Fig. 5 for $R = 0.1$ and in Fig. 6 for $R = 0.4$. Likewise, Figs. 7 and 8

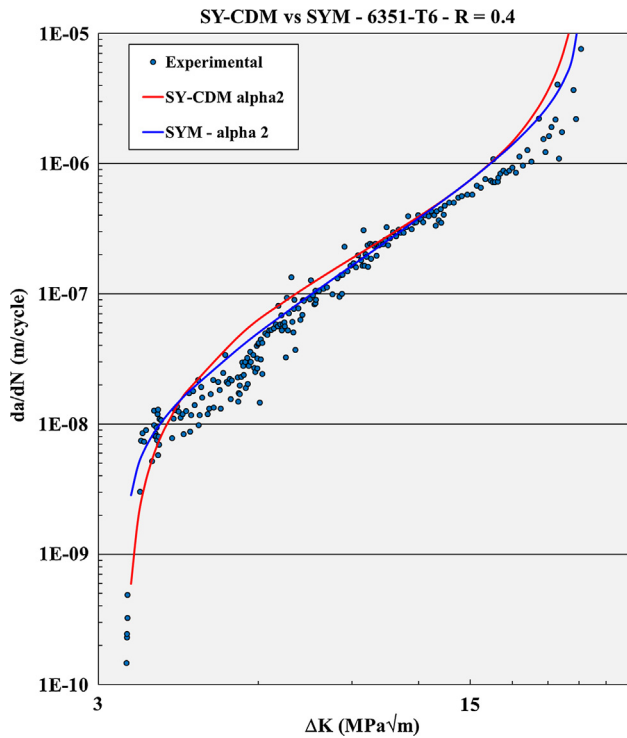


Fig. 12. SY-CDM and SYM predictions for the $da/dN \times \Delta K$ curve of the 6351-T6 alloy at $R = 0.4$, compared with the experimental data measured according to ASTM E647 procedures.

present the predictions for 7075-T6 Al alloy, and Figs. 9 and 10 for 1020 low carbon steel.

The elimination of crack closure (by artificially forcing $K_{op} = 0$) results in significant FCG rate increments for almost all simulation conditions. This of course indicates that K_{op} effects should not be neglected in practical applications. Crack closure effects on FCG rates follow the same tendency for the three materials, i.e. they are higher for plane stress conditions (where $\alpha = 1$) and for $R = 0.1$. However, the FCG modelling approach based on the ΔK_{eff} hypothesis is much more sensitive to the K_{op} value than the critical damage approach. This is not a surprise, due to the direct dependence of ΔK_{eff} on K_{op} . Table 3 presents the average FCG rate increment for each simulated condition listed in Table 1. It lists as well the ratio between the rates predicted by the SYM (using its ΔK_{eff} -based approach) and by the SY-CDM (considering K_{op} effects on the strain ranges ahead of the crack tip). For $\alpha = 1$ and for $R = 0.1$ e.g. this ratio is 2.9 for the 6351-T6 and 6.2 for the 7075-T6 Al alloys, and 4.0 for the 1020 steel. Notice how much more sensitive the predictions based on ΔK_{eff} are to K_{op} than the CDM predictions, a point that can help identifying the actual FCG driving forces in practical problems.

Indeed, Table 3 shows that the increases in FCG rates predicted by the SYM assuming ΔK_{eff} is the FCG driving force are always much

higher than the ϵN -based SY-CDM predictions when K_{op} is neglected. The SYM assumes there is no damage ahead of the crack tip while it is closed under loads $K < K_{op}$. Therefore, when K_{op} is forced to be null, it predicts large ΔK_{eff} changes and thus large FCG rate increases. The SY-CDM, on the other hand, uses the cyclic plastic strains ahead of the crack tip induced by the whole range of applied load as the FCG driving force, considering as well the effect of crack closure by keeping residual plastic deformations at the crack wake.

Hence, Table 3 shows that SYM ΔK_{eff} -based predictions overestimate the effect of crack closure in comparison to the $\Delta \epsilon$ -based SY-CDM predictions. This is once again not a surprise, since there is plenty of evidence collected by ΔK_{eff} supporters indicating that ΔK_{eff} -based FCG rate predictions can overestimate crack closure effects. For instance, Donald and Paris [38], testing 6061-T6 and 2024-T3 Al alloy specimens, concluded that the method used to calculate ΔK_{eff} proposed by Elber [2] was not appropriate to describe their results, since it overestimated the crack closure effect measured in their tests.

Similar evidence about the actual effect of crack closure came from the work of Hertzberg et al. [39]. They tested 7 mm thick Al-Cu-0.7Si Al alloy and 9 mm thick 4340 steel specimens, and studied the effect of artificially increasing K_{op} by using 50, 75, and 100 μm thick shims between the crack faces. For Al alloy, e.g., K_{op} increased from 13% to 30%, 50%, and 93% of K_{max} , while FCG rates reduced by a factor of 1.2, 2.7, and 4.7. However, if really caused by ΔK_{eff} , FCG rates should have reduced by much larger factors (16, 27, and 800, respectively), not by the values reported by the authors. It is interesting to note that those authors did not question the basic “ ΔK_{eff} is the FCG driving force” idea in view of their own results, an evidence that the overestimation of the FCG rates they measured in their tests was not biased in any way.

It is important to emphasize that even though SYMs and SY-CDMs use completely different philosophies to estimate FCG rates, both can reproduce quite well $da/dN \times \Delta K$ curves of several materials, as previously studied in [31–33]. These works compare their predictions for the 7075-T6 Al alloy and for the 1020 steel with experimental data. Similar new data presented in Figs. 11 and 12 for the $da/dN \times \Delta K$ curves of the 6351-T6 Al alloy at $R = 0.1$ and $R = 0.4$ support this claim.

However, besides the difference between the crack driving forces assumed by each model, it is important to emphasize as well that SY-CDMs calculate FCG rates directly from the accumulated damage using ϵN procedures that do not need or use any data-fitting parameter to describe the experimental $da/dN \times \Delta K$ results. This is certainly a major asset of such models.

The SYM, on the other hand, uses a pre-chosen Forman-Newman FCG rule to predict its da/dN rates, which has four data-fitting parameters (not to mention that the transversal constraint α is frequently used as a 5th data-fitting parameter in most practical applications). These parameters must be found by adjusting the rule to a suitable set of experimental FCG data. Hence, even though Elber’s hypothesis overestimates the effect of crack closure, the numerous SYM data-fitting parameters allow it to reproduce $da/dN \times \Delta K$ curves quite reasonably (if α is properly chosen), as well as to perform acceptable residual life predictions in many practical cases. Nevertheless, reasonable

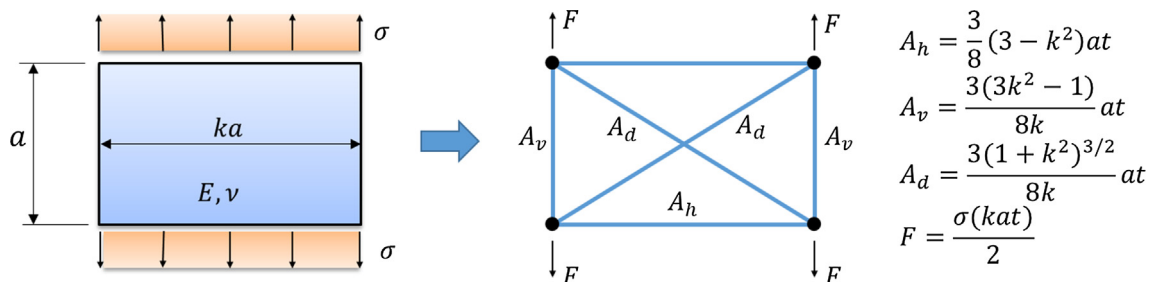


Fig. 13. Bar elements for plane stress [40] to represent 2D continuous solid.

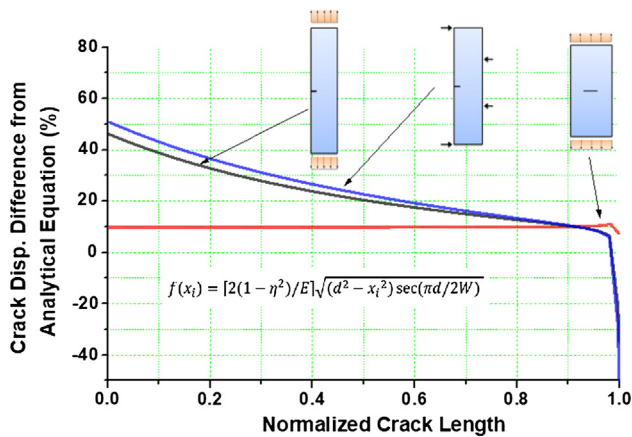


Fig. 14. Crack displacement differences considering the analytical Eq. (2).

predictions resulting from the five properly calibrated data-fitting parameters do not prove that ΔK_{eff} is the actual FCG driving force. In fact, if the SY-CDM can match the SYM predictions using no data-fitting parameters, from Occam's razor principle it at least deserves to be considered as a viable option for practical applications, not to mention as a promising tool for basic fatigue research.

These analyses indicate that further experimental verifications of the actual FCG driving force should always be supported by suitable K_{op} measurements. In fact, Kemp pointed out this need a long time ago [40]. In other words, if ΔK_{eff} has indeed a tendency to overestimate fatigue crack closure effects, it should be properly measured in all evaluations based on SYM predictions, even if it can be properly fitted to the experimental data.

Finally, although the above approximation presents satisfactory results, it is possible to improve the model to better characterize the actual material behavior. Three improvements can be suggested here: (i) to improve the description of the material behavior by its cyclic fatigue properties using better constitutive models; (ii) to add bar elements to represent strain constraints in the continuum solid; and (iii) to improve displacement equations for the crack faces.

The first improvement is obvious, because the cyclic constitutive model used here assumes the material is perfectly plastic, a rudimentary approximation. The second can be to use, for example, the pattern of bars proposed by Nagarajan et al. [41] that exhibits the same deformation behavior of the continuum solid (assuming $\nu = 1/3$ and plane stress), as illustrated in Fig. 13. The strip-yield model assumes the bar elements are independent of each other, so they do not represent the transverse deformations resulting from the Poisson effect, neither the plastic deformation constraints induced by them. The third improvement can solve the problem of the crack face displacement given by Eq. (2) being limited to a specific situation of geometry and boundary conditions. For instance, Fig. 14 shows differences of crack face displacements for three different geometries and boundary conditions with the same FIT for a crack size to width ratio $a/w = 0.2$. Notice how that the crack opening can have significant differences for different geometries, which could be accounted for if better modeled in the SYMs and thus in the SY-CDMs as well. However, none of these improvements has been introduced here to avoid masking the intended comparisons between SYM and SY-CDM predictions, since the main objective of this work is to evaluate the K_{op} effect on ΔK_{eff} and on the damage field ahead of the crack tip according to the traditional SYM mechanics. However, such improvements will certainly be explored in future works.

5. Conclusions

SYM and SY-CDM predictions for several materials (6351-T6 and 7075-T6 Al alloys, and 1020 steel) indicate that the influence of crack

closure on FCG rates can be significantly lower when modeled by damage accumulation principles than when accounted by assuming ΔK_{eff} is the FCG driving force. Indeed, SY-CDMs predictions, which assume FCG rates are caused by the damage accumulated by the strain range distribution ahead of the crack tip, predict much lower (although significant) K_{op} effects than ΔK_{eff} -based crack SYMs predictions. This comparison is coherent since even though SY-CDMs predictions do not use ΔK_{eff} concepts, they do consider crack closure effects because they are based on the very same strip-yield mechanics used by the SYMs. Hence, if ΔK_{eff} has indeed a tendency to overestimate fatigue crack closure effects, this can be an evidence it may not be the FCG driving force. In any case, to allow the correct identification of the true FCG driving force, K_{op} should be properly measured in all experimental verifications of FCG predictions, even if they can be properly fitted to the measured data.

References

- [1] Elber W. Fatigue crack closure under cyclic tension. *Eng Fract Mech* 1970;2:37–45.
- [2] Elber W. The significance of fatigue crack closure. *Damage tolerance in aircraft structures ASTM STP*. 1971. p. 230–42.
- [3] Machniewicz T. Fatigue crack growth prediction models for metallic materials – part I: overview of prediction concepts. *Fatigue Fract Eng Mat Struct* 2012;36:293–307.
- [4] Willenborg JD, Engle RM, Wood HA. A crack growth retardation model using an effective stress concept. AFFEL-TM-71-1-FBR, Wright Patterson Air Force Laboratory. 1971.
- [5] Wheeler OE. Spectrum loading and crack growth. *J Basic Eng* 1972;94:181–6.
- [6] Dill HD, Saff CR. Spectrum crack growth prediction method based on crack surface displacement and contact analyses. *Fatigue crack growth under spectrum loads ASTM STP*. 1976. p. 306–19.
- [7] Newman Jr JC. A crack-closure model for predicting fatigue crack growth under aircraft spectrum loading. *Methods and models for predicting fatigue crack growth under random loading ASTM STP*. 1981. p. 53–84.
- [8] Newman Jr JC. Prediction of fatigue crack growth under variable-amplitude and spectrum loading using a closure model. *Design of fatigue and fracture resistant structures ASTM STP*. 1982. p. 255–77.
- [9] Newman Jr JC. FASTRAN II: a fatigue crack growth structural analysis program. NASA Technical Memorandum 104159 LRC Hampton. 1992.
- [10] Newman Jr JC. FASTRAN: a fatigue crack growth life-prediction code based on the crack-closure concept – version 5.4. *Fatigue and Fracture Associates North Lake Circle*. 2013.
- [11] De Koning AU, Liefing G. Analysis of crack opening behavior by application of a discretized strip yield model. *Mechanics of Fatigue Crack Closure, ASTM STP*. 1988. p. 437–58.
- [12] Wang GS, Blom AF. A strip model for fatigue crack growth predictions under general load conditions. *Eng Fract Mech* 1991;40:507–33.
- [13] Beretta S, Carboni M. A strip-yield algorithm for the analysis of closure evaluation near the crack tip. *Eng Fract Mech* 2005;72:1222–37.
- [14] Machniewicz T. Fatigue crack growth prediction models for metallic materials – part II: strip yield model – choices and decisions. *Fatigue Fract Eng Mat Struct* 2012;36:361–73.
- [15] Majumdar S, Morrow JD. Correlation between fatigue crack propagation and low cycle fatigue properties. *Fracture Toughness Slow-Stable Cracking, ASTM STP*. 1974. p. 159–82.
- [16] Glinka G. A notch stress-strain analysis approach to fatigue crack growth. *Eng Fract Mech* 1985;21:245–61.
- [17] Castro JTP, Kenedi PP. Prediction of fatigue crack growth rates departing from Coffin-Manson concepts. *J Braz Soc Mech Sci Eng* 1995;17:292–303. (in Portuguese).
- [18] Durán JAR, Castro JTP, Payão Filho JC. Fatigue crack propagation prediction by cyclic plasticity damage accumulation models. *Fatigue Fract Eng Mater Struct* 2003;26:137–50.
- [19] Noroozi AH, Glinka G, Lambert S. A study of the stress ratio effects on fatigue crack growth using the unified two-parameters fatigue crack growth driving force. *Int J Fatigue* 2007;29:1616–34.
- [20] Castro JTP, Meggiolaro MA, Miranda ACO. Fatigue crack growth predictions based on damage accumulation calculations ahead of the crack tip. *Comput Mat Sci* 2009;46:115–23.
- [21] Dugdale DS. Yielding of sheets containing slits. *J Mech Phys Solids* 1960;8:100–4.
- [22] Barenblatt GI. The mathematical theory of equilibrium cracks in brittle fracture. *Adv Appl Mech* 1962;7:55–192.
- [23] Kemp PMJ. Fatigue crack closure – a review. Royal Aerospace Establishment: TR90046. 1990.
- [24] Williams JJ, Yazzie KE, Padilla E, Chawla N, Xiao X, de Carlo F. Understanding fatigue crack growth in aluminum alloys by in situ X-ray synchrotron tomography. *Int J Fatigue* 2013;57:79–85.
- [25] Castro JTP, Meggiolaro MA, Miranda ACO. Singular and non-singular approaches for predicting fatigue crack growth behavior. *Int J Fatigue* 2005;27:1366–88.
- [26] Vasudevan AK, Sadananda K, Louat N. A review of crack closure, fatigue crack

- threshold and related phenomena. *Mater Sci Eng* 1994;188A:1–22.
- [27] Toyosada M, Niwa T. The significance of RPG load for fatigue crack propagation and the development of a compliance measuring system. *Int J Fract* 1994;67:217–30.
- [28] Chen DL, Weiss B, Stickler R. The effective fatigue threshold: significance of the loading cycle below the crack opening load. *Int J Fatigue* 1994;16:485–91.
- [29] Vasudevan AK, Sadananda K, Holtz RL. Analysis of vacuum fatigue crack growth results and its implications. *Int J Fatigue* 2005;27:1519–29.
- [30] Castro JTP, Meggiolaro MA, González JAO. Can ΔK_{eff} be assumed as the driving force for fatigue crack growth? *Frattura ed Integrità Strutturale* 2015;33:97–104.
- [31] Ferreira SE, Castro JTP, Meggiolaro MA. Using the strip-yield mechanics to model fatigue crack growth by damage accumulation ahead of the crack tip. *Int J Fatigue* 2017;103:557–75.
- [32] Ferreira SE, Castro JTP, Meggiolaro MA. A model to quantify fatigue crack growth by cyclic damage accumulation calculated by strip-yield procedures. *Frattura ed Integrità Strutturale* 2017;41:129–38.
- [33] Ferreira SE, Castro JTP, Meggiolaro MA. Fatigue crack growth predictions based on damage accumulation ahead of the crack tip calculated by strip-yield procedures. *Int J Fatigue* 2018;115:89–106.
- [34] NASA, Southwest Research Institute. NASGRO: Fracture Mechanics and Fatigue Crack Growth Analysis Software, Reference Manual, version 4.02; 2002.
- [35] Ferreira SE, Castro JTP, Meggiolaro MA. A strip-yield algorithm to predict fatigue crack closure and growth. 24th ABCM Int. Congress of Mechanical Engineering Curitiba-PR. 2017.
- [36] Rice JR. Mechanics of crack tip deformation and extension by fatigue. *Fatigue Crack Propagation*, ASTM STP. 1967. p. 247–311.
- [37] James MN, Knott JF. An assessment of crack closure and the extent of the short crack regime in Q1N (HY80) steel. *Fatigue Fract Eng Mater Struct* 1985;8:177–91.
- [38] Donald K, Paris PC. An evaluation of ΔK_{eff} estimation procedures on 6061-T6 and 2024-T3 aluminum alloys. *Int J Fatigue* 1999;21:47–57.
- [39] Hertzberg RW, Newton CH, Jaccard R. Crack closure: correlation and confusion. *ASTM STP* 1988;982:139–48.
- [40] Kemp PMJ. Fatigue crack closure – a review. TR90046, Royal Aerospace Establishment, UK. 1990.
- [41] Nagarajan P, Jayadeep UB, Madhavan Pillai TM. Application of micro truss and strut and tie model for analysis and design of reinforced concrete structural elements. *Songklanakarin J Sci Technol* 2009;31(6):647–53.